Received: 21 October 2023 | Revised: 22 February 2024 | Accepted: 2 April 2024

DOI: 10.1111/apha.14146

ACTA PHYSIOLOGICA

RESEARCH PAPER

The homeostatic effects of the RE-1 silencing transcription factor on cortical networks are altered under ictogenic conditions in the mouse

Carmela Vitale[1,2] | Giulia Natali[1,3] | Maria Sabina Cerullo[1,3] | Thomas Floss[4] | Caterina Michetti[1,3] | Giorgio Grasselli[2,5] | Fabio Benfenati[1,2]

[1]Center for Synaptic Neuroscience and Technology, Istituto Italiano di Tecnologia, Genova, Italy

[2]IRCCS Ospedale Policlinico San Martino, Genova, Italy

[3]Department of Experimental Medicine, University of Genova, Genova, Italy

[4]Helmholtz Zentrum München, Deutsches Forschungszentrum für Gesundheit und Umwelt, Neuherberg, Germany

[5]Department of Pharmacy, University of Genova, Genova, Italy

Correspondence
Fabio Benfenati, Center for Synaptic Neuroscience and Technology, Istituto Italiano di Tecnologia, Largo Rosanna Benzi, 10 - 16132 Genova, Italy.
Email: fabio.benfenati@iit.it

Funding information
Ministero della Salute; Ministero dell'Università e della Ricerca; Compagnia di San Paolo; IRCCS Ospedale Policlinico San Martino

Abstract

Aim: The Repressor Element-1 Silencing Transcription Factor (REST) is an epigenetic master regulator playing a crucial role in the nervous system. In early developmental stages, REST downregulation promotes neuronal differentiation and the acquisition of the neuronal phenotype. In addition, postnatal fluctuations in REST expression contribute to shaping neuronal networks and maintaining network homeostasis. Here we investigate the role of the early postnatal deletion of neuronal REST in the assembly and strength of excitatory and inhibitory synaptic connections.

Methods: We investigated excitatory and inhibitory synaptic transmission by patch-clamp recordings in acute neocortical slices in a conditional knockout mouse model (*Rest*^{GTi}) in which *Rest* was deleted by delivering PHP.eB adeno-associated viruses encoding CRE recombinase under the control of the human synapsin I promoter in the lateral ventricles of P0-P1 pups.

Results: We show that, under physiological conditions, *Rest* deletion increased the intrinsic excitability of principal cortical neurons in the primary visual cortex and the density and strength of excitatory synaptic connections impinging on them, without affecting inhibitory transmission. Conversely, in the presence of a pathological excitation/inhibition imbalance induced by pentylenetetrazol, *Rest* deletion prevented the increase in synaptic excitation and decreased seizure severity.

Conclusion: The data indicate that REST exerts distinct effects on the excitability of cortical circuits depending on whether it acts under physiological conditions or in the presence of pathologic network hyperexcitability. In the former case, REST preserves a correct excitatory/inhibitory balance in cortical circuits, while in the latter REST loses its homeostatic activity and may become pro-epileptogenic.

KEYWORDS

epilepsy, REST conditional knockout, REST/NRSF, seizure propensity, synaptic transmission

Carmela Vitale and Giulia Natali contributed equally to this work.

1 | INTRODUCTION

The repressor element-1 silencing transcription factor (REST), also known as neuron-restrictive silencer factor, is an epigenetic master regulator. Upon binding to a 21 base pair sequence called repressor element-1 (RE-1) or neuron-restrictive silencer element (NRSE), REST recruits and coordinates several chromatin-modifying enzymes acting mainly as transcriptional repressor.[1] RE-1 sequences are present in single or multiple copies in the promoter regions of numerous neuron-specific genes encoding ion channels, neurotransmitters, proteins involved in axonal guidance, vesicle trafficking and fusion where it exerts transcriptional inhibition.[2] In line with this, REST downregulation plays a key role in mastering the acquisition of the neuronal phenotype during embryonal development. At first, REST levels are highest in the nuclei of pluripotent stem cells. Then, during transition to neural progenitors, the REST protein levels dramatically decrease because of post-translational degradation.[3]

Further studies demonstrated that REST in not only a switch for neuronal fate but is also critical for the fine-tuning of synaptic connectivity and plasticity of neuronal networks during critical periods.[4] REST modulation participates in the upregulation of the potassium chloride transporter 2 (KCC2) in the perinatal period controlling the timing of the chloride shift[5] fundamental for the establishment of GABAergic inhibitory transmission.[6,7] Moreover, in postnatal neurons REST regulates the subunit switch in N-methyl-D-aspartate (NMDA) receptors that, between P15 and P17 in rats, replaces the GluN2B subunits present during early postnatal development with the GluN2A subunit.[8,9]

In addition to these developmental roles, REST is also involved in controlling changes in neuronal networks in response to stress. While behavioral responses to stress can mostly reverse quickly, epigenetic changes to the chromatin structure can last longer.[10] REST has been reported to mediate homeostatic protection from network hyperexcitability, by constraining the expression of voltage-gated sodium channels[11] and excitatory synaptic transmission.[12] Moreover, it has been recently demonstrated that REST increases the strength of axo-somatic inhibitory synapses onto excitatory neurons, while having no effect when the postsynaptic target cell was another inhibitory neuron.[13] A similar homeostatic effect was recently observed in astrocytes, where REST increases the transcription of the glutamate transporter GLT1 and favors the membrane exposure of the potassium channel Kir4.1, thus increasing glutamate and potassium clearance from the synaptic environment.[14]

Notwithstanding these effects, the understanding of the role of REST in shaping neuronal networks is still largely incomplete, especially in the first phases of postnatal development. Hence, we here investigate the role of REST in shaping the neocortical excitatory/inhibitory (E/I) networks in the mouse early postnatal period under physiological conditions and test its activity under conditions of excitation/inhibition imbalance. To this aim, we deleted REST specifically in neurons in vivo in a conditional knockout mouse strain (*Rest*^{GTi}) by using a modified AAV vector encoding CRE under the control of the pan-neuronal human synapsin I (*hSyn1*) promoter packaged in an engineered viral capsid with increased transduction efficiency and biological barrier penetration (PHP.eB). Ex vivo whole-cell patch-clamp recordings and immunochemical mapping of excitatory and inhibitory synaptic contacts showed that *Rest* deletion under physiological conditions imbalances cortical synaptic balance in favor of excitatory inputs to principal neurons, identifying REST as a homeostatic factor that maintains a correct E/I balance during the development of cortical networks. On the contrary, under conditions of network hyperexcitability, *Rest* deletion prevents the rise of excitatory strength, switching the REST action from homeostatic to pro-epileptogenic.

2 | METHODS

All the material submitted is conform with good publishing practice in physiology and the *Acta Physiologica* guidelines.[15]

2.1 | Animals

Wild-type C57BL/6J male mice were purchased from Charles River (Calco, Italy). GTinv*Rest* mice (*Rest*^{GTi} mice[16]) were obtained by Gail Mandel (Portland, OR) and the German Gene Trap Consortium (GGTC Partners) and kept on a C57BL/6J background in homozygosity under conditions of environmental enrichment. Mice were maintained on a 12:12 h light/dark cycle at constant temperature (22 ± 1°C) and humidity (60 ± 10%), with water and pellet diet ad libitum. All the experiments were strictly following the guidelines of the European Community Council (Directive 2014/63/EU of 15 May 2014) and were approved by the Italian Ministry of Health (Authorization #558/2016-PR and #427/2021-PR).

2.2 | Plasmid cloning

The *hSyn1* minimal promoter was amplified by PCR from phSyn1-GFP-C1-Flag using hSyn1-specific primers

(hSyn1-FW and hSyn1-RV; see below for sequences). The isolated promoter was cloned in pAAV-CAG-NLSx2-GFP,[17] replacing the CAG promoter. Sequences corresponding to either Cre recombinase or a recombinase-dead Cre mutant (ΔCre; Cre deleted at residues 134–343 in the catalytic domain), used as a negative control, were PCR-amplified from pLenti-PGK-Cre-GFP and pLenti-PGK-ΔCre-GFP,[18] respectively. Isolated Cre and ΔCre sequences were digested and cloned in the intermediate plasmid carrying the *hSyn1* promoter. The used primers were:

hSyn1-FW: 5′-atccactagtctgcagagggccctgcg-3′;
hSyn1-RV: 5′-atccgcggccgcgcgccgcagcgcagatgg-3′;
ΔCre and Cre-FW: 5′-atccgcggccgccaccatggtgaagcgacc-3′;
ΔCre-RV: 5′-atccggatccctacttacggattcgccgc-3′;
Cre-RV: 5′-atccttaattaactaatcgccatcttccagcag-3′;
Oligo containing Pac1-FW: 5′-gatccatatgttaattaaggcgcg cccaattg-3′;
Oligo containing Pac1-RV: 5′-gatccaattgggcgcgccttaatt aacatatg-3′.

2.3 | AAV production

After checking the integrity of the ITR AAV2 packaging signals, AAV1/2 viral particles containing pAAV-hSyn1-NLSx2-GFP were generated as previously described.[19] Viruses were purified over heparin columns (GE HealthCare Life Science, Milano, Italy) at a concentration of $1–10\times10^{11}$ vector genomes (vg)/mL and used at a multiplicity of infection of 10 000. The infection efficiency was 70%–90%. pAAV-hSyn1-NLS-GFP- ΔCRE/CRE were packaged into PHP.eB capsids by Vector Biolabs (Malvern, PA).

2.4 | Assessment of targeting specificity in adult mice

Two/three-month-old *Rest*^{GTi} mice were stereotaxically injected in the cerebral cortex (AP-1.46 mm, L 3 mm, DV 1.5 mm) with 1 μL of 10^9 vg/mL AAV1/2 hSyn1-NLS-GFP-ΔCRE/CRE particles delivered at 0.1 μL/min under anesthesia with 1%–3% isoflurane (0.8–1.5 L/min). After surgery, analgesics (ketoprofen 0.5–1 mg/kg; dexamethasone 5 mg/kg) were administered intraperitoneally.

2.5 | Intraventricular injections in pups

After inducing anesthesia with hypothermia, P0/P1 *Rest*^{GTi} pups were injected in the lateral ventricles with PHP.eB hSyn1-NLS-GFP-ΔCre/Cre particles. The injection site was located at about 2/5 of the distance between the lambda suture and the eye. We held a glass capillary at a depth of 3 mm and perpendicular to the pup skull and injected 2 μL of virus and Fast Green dye (1:100; 2353-45-9, Merck-Millipore, Darmstadt, Germany) into each ventricle. After the procedure, pups were laid under the heating lamp to recover from anesthesia.

2.6 | Immunofluorescence

Rest^{GTi} mice, previously injected with either AAV1/2 hSyn1-NLSx2-GFP or PHP.eB hSyn1-NLS-GFP-ΔCre/Cre, were transcardially perfused under deep anesthesia with ice-cold phosphate-buffered saline (PBS), followed by 4% paraformaldehyde in PBS.

2.6.1 | Immunofluorescence

Brains were dissected, post-fixed overnight at 4°C, cryoprotected in 30% sucrose solution, cut in 30 μm sections with a Vibratome (Leica, Wetzlar, Germany) and processed for immunofluorescence as previously described.[20] The primary antibodies were: guinea pig anti-green fluorescent protein (GFP; 1:500, Synaptic Systems, Göttingen, Germany), rabbit anti-green fluorescent protein (GFP; 1:500, Synaptic Systems), mouse anti-neuronal nuclear antigen (NeuN; 1:500, Merck), guinea pig anti-glial fibrillary acidic protein (GFAP; 1:500, Synaptic Systems), guinea pig anti-ionized calcium-binding adapter molecule 1 (Iba1; 1:500, Synaptic Systems), rabbit anti-vesicular GABA transporter (VGAT; 1:250, Synaptic Systems), guinea pig anti-vesicular glutamate transporter-1 (VGLUT1; 1:250, Synaptic Systems), mouse anti-gephyrin (1:1000, Synaptic Systems), and mouse anti-postsynaptic density protein 95 (PSD-95; 1:1000, Thermo-Fisher Scientific). After the incubation with primary antibodies, sections were stained with secondary antibodies (anti-guinea pig Alexa Fluor 488 and 647, anti-rabbit Alexa Fluor 488 and 568, anti-mouse Alexa Fluor 568 and 647; Invitrogen, Waltham, MA) and the nuclear stain Hoechst 34580 (Thermo-Fisher Scientific). Sections were observed with as SP8 confocal fluorescence microscope and a 63× oil immersion objective (Leica, Wetzlar, Germany).

2.6.2 | Promoter specificity and efficiency of transduction

GFP positive (GFP^+) and specifically labeled cell types were analyzed using ImageJ to determine promoter specificity (cell type-specific GFP^+ cells in percent of the

total GFP^+ cells) and penetrance (cell type-specific GFP^+ cells in percent of the total cell type-specific population). For the assessment of the AAV transduction efficiency, the entire slices were imaged by merging single acquisitions (20× objective) to automatically count $Hoechst^+$ and GFP^+ cell profiles using ImageJ. The AAV transduction efficiency was expressed as the ratio between GFP^+ cells over the total number of Hoechst+ profiles.

2.6.3 | Synaptic density

For each brain slice, serial optical sections were acquired with a 63× oil immersion objective at 0.33 µm intervals over a total depth of 5 µm for a total of 15 optical sections. Maximum intensity projections (MIPs) were generated from groups of three consecutive sections yielding five MIPs representing 1 µm of depth each. Double-positive $vGAT^+$/$Gephyrin^+$ or $vGLUT1^+$/$PSD\text{-}95^+$ puncta were counted in an automated fashion with the ImageJ software ("Analyze particles" function) and their density was expressed as puncta/mm^3.

2.7 | In vivo treatment with pentylenetetrazol

Rest^{GTi} mice, previously injected with PHP.eB hSyn1-NLS-GFP-ΔCRE/CRE, were subjected to treatment with pentylenetetrazol (PTZ) at P30-P40. PTZ (Merck-Millipore) was dissolved in saline and administered intraperitoneally at a dose of 60 mg/kg for 2 days on alternate days. After the injection, mice were single-housed, videotaped for 30 min or until death occurred and scored according to a modified Racine scale (0, normal behavior; 1, immobility; 2, twitch; 3, Straub's tail; 4, mild seizure; 5, tonic–clonic seizure; 6, death).[21]

2.8 | Electrophysiology in acute brain slices

Rest^{GTi} mice, previously injected with the viral vectors at P0/P1, were deeply anesthetized at P30-40 with CO_2 and sacrificed by cervical dislocation. Brains were immediately transferred in an ice-cold dissecting artificial cerebrospinal fluid (aCSF1) containing (in mM): 100 NaCl, 2.5 KCl, 1.25 NaH_2PO_4, 25 $NaHCO_3$, 5 sodium ascorbate, 3 sodium pyruvate, 25 D-Glucose, 10 $MgSO_4$, and 0.5 $CaCl_2$ (300 mosm/L), bubbled with 95% O_2 and 5% CO_2, pH 7.4. Coronal slices (300 µm thick) were obtained using a vibratome VT1200 S (Leica) in ice-cold aCSF1. After sectioning, slices were stored for 30 min at 33°C in aCSF1, then at RT for ≥30 min before being transferred to the recording chamber. Whole-cell patch-clamp recordings were performed in a submerged chamber at 30 ± 1°C with at a constant flow (2 mL/min) of recording artificial cerebrospinal fluid (aCSF2) containing (in mM): 120 NaCl, 2.5 KCl, 1.25 NaH_2PO_4, 25 $NaHCO_3$, 12.5 Glucose, 1.5 $MgSO_4$, 2.5 $CaCl_2$ (300 mosm/L), bubbled with 95% O_2 and 5% CO_2, pH 7.4. Glass micropipettes (3–5 MΩ) were filled with an internal solution containing (in mM): 110 KGluconate, 20 KCl, 5 NaCl, 10 Hepes, 0.5 EGTA, 1 $MgCl_2$, 4 MgATP, 0.5 NaGTP, 20 Na_2CreatinineP (290 mOsm/L), pH 7.3. All recordings were obtained from GFP^+ pyramidal neurons in layer 2/3 of the primary visual cortex (V1), visually identified based on their pyramidal shape and firing pattern.[22] Before starting each experiment, the resting membrane potential (V_m) was measured immediately after breaking the membrane and establishing the whole-cell mode. Neurons with $V_m > -58$ mV were discarded. All protocols included a 100 ms-long hyperpolarizing step of −5 mV to estimate the passive properties of the neurons: input resistance (R_{in}), series resistance (R_s), and membrane capacitance (C_m). Series resistance was monitored at regular intervals throughout the measurements and only recordings with low (≤25 MΩ) and stable series resistance were included in the study (≤20% change). No series resistance compensation and corrections for liquid junction potentials were made. Only c-fast was compensated for the membrane capacitance. Only cells with a stable resting membrane potential throughout the current-clamp protocols were included in the analysis.

Current-clamp experiments were performed in the presence of inhibitors of AMPA receptors (CNQX, 10 µM), $GABA_A$ receptors (picrotoxin, 100 µM), NMDA receptors (D-APV, 100 µM), $GABA_B$ receptors (CGP35348, 5 µM). Current injections were performed with a duration of 1 s and increasing in amplitude from 0 to 400 pA with 20 pA current steps to elicit action potentials and estimate the firing threshold. In current-clamp experiments, data were sampled at 50 kHz and low-pass filtered at 5 kHz. To analyze the shape of the action potential the data were sampled at 50 kHz and filtered at 10 kHz. To study the biophysical properties of the single AP, the plot of the time derivative of voltage (dV/dt) versus voltage was obtained (phase-plane plot) from the first AP elicited by the minimal current injection was used to extract the V threshold (defined as the first voltage at which the voltage rate exceeds 5 mV/ms), AP peak, rising slope, falling slope, trough, and width were extracted from the individual phase-plane plots.[22,23]

Spontaneous excitatory postsynaptic currents (sEPSCs) were acquired in the voltage-clamp configuration with the membrane potential clamped at −50 mV in the presence of only picrotoxin and D-APV. Miniature excitatory postsynaptic currents (mEPSC) were recorded

at −50 mV with the addition of tetrodotoxin (TTX, 1 μM). Spontaneous inhibitory postsynaptic current (sIPSC) were recorded at −40 mV in the presence of CNQX (10 μM) and D-APV (100 μM) in the bath, using a low Cl^- intracellular solution containing (in mM): 150 KGluconate, 1 KCl, 5 NaCl, 10 Hepes, 0.5 EGTA, 4 MgATP, 0.5 NaGTP, 20 Na_2CreatinineP (290 mOsm/L), pH 7.3. TTX (1 μM) was added to the bath for miniature inhibitory postsynaptic current (mIPSC) recordings. In the voltage-clamp mode, data were filtered at 5 kHz and sampled at 50 kHz. Data were acquired using a triple patch-clamp EPC10 USB amplifier (HEKA, Lambrecht Germany) and stored using the Patchmaster (v2 × 73.1) software. pCLAMP 10 (Axon) and MATLAB were used to analyze current-clamp experiments. MiniAnalysis (Synaptosoft Inc., USA) to analyze sEPSCs, mEPSCs, sIPSCs, and mIPSCs. Postsynaptic events were identified using a peak detector function using appropriate threshold amplitude (5pA) and threshold area (20 ms * pA) for EPSCs and IPSCs. The amplitude of PSCs was measured as the difference between the baseline and the peak. The frequency of PSCs was calculated by counting the number of PSC events within 4 min. The PSC 10%–90% rise time was considered as the time taken for the PSC to rise from 10% to 90% of its peak amplitude, whereas the PSC decay time was considered as the time taken for the PSC to decay to 20% of its peak amplitude.

2.9 | Statistics

Data are reported as means ± standard error of the mean (SEM). The Shapiro–Wilk test was used to check for normal distribution. The unpaired Student's *t*-test was used to compare two normally distributed samples. To compare experimental groups, one-way, two-way, or two-way repeated measures ANOVA followed by the Tukey test was used to compare more than two normally distributed samples. The Kolmogorov–Smirnov and the Fisher exact tests were used to assess cumulative curves and contingency, respectively. The significance level was fixed at $p < 0.05$. GraphPad Prism 8 software (GraphPad Software Inc., San Diego, CA, USA) was used for statistics and graphs.

3 | RESULTS

3.1 | Induction of neuron-specific knockout of REST

To knockout REST specifically in neurons, we designed AAV vectors encoding the CRE recombinase under a neuron-specific promoter. To cope with the limited AAV cargo capacity (4.7 kb),[24] we chose the minimal promoter *hSyn1* (405 bp) able to ensure the transcription start and the cellular and tissue specificity.[25] First, we replaced the ubiquitous CAG promoter located in the pAAV-CAG-NLSx2-GFP plasmid with the minimal promoter. We then cloned the sequence encoding the CRE recombinase or its inactive deletion mutant form (ΔCre) fused with a nuclear green fluorescent protein (nGFP), in place of the original GFP sequence (Figure 1A).

We firstly verified the efficiency and specificity of the minimal promoter by packaging the hSyn1-NLSx2-GFP vector plasmid into AAV1/2 capsids that were stereotaxically injected in the neocortex of 2-month-old *Rest*^{GTi} mice. In immunofluorescently labelled brain sections obtained 4 weeks after the injection (Figure 1B), we analyzed the cell-specific expression as the fraction of GFP^+ cells positive for the neuron-specific marker NeuN (compared with other cell type-specific markers; Figure 1D) and the penetrance of GFP expression as the fraction of neurons expressing GFP (compared with other cell types; Figure 1E). The hSyn1 minimal promoter showed an almost complete specificity for $NeuN^+$ neuronal cells (94.20 ± 0.55%; $n = 3$ mice) and almost undetectable expression in $GFAP^+$ astroglial cells (0.50 ± 0.25%) and $Iba1^+$ microglial cells (0.23 ± 0.12%) cells (Figure 1D). Penetrance was highest in neurons (70.53 ± 4.10%), while negligible transduction was detected in astroglia (3.60 ± 2.27%) and microglia (0.93 ± 0.46%).

For the following experiments, aimed at generating widespread REST knockout in the developing postnatal brain, hSyn1-NLS-GFP-ΔCRE/CRE vectors were packaged into capsid-engineered AAV-PHP.eB, which provide improved transduction efficiency, barrier crossing and higher diffusion throughout the tissue.[17] By injecting these viral particles in the lateral ventricles of *Rest*^{GTi} mice pups, we observed that the expression of the reporter reached an optimal transduction in the primary visual cortex (V1) 4 weeks after the injection (Figure 1H; 1st wk: 24.89 ± 1.95%; 2nd wk: 28.48 ± 1.39%; 3rd wk: 35.45 ± 2.85%; 4th wk: 47.87 ± 2.91%).

3.2 | *Rest*-KO pyramidal neurons in layers II/III of the V1 cortex display higher intrinsic excitability

The effects of the pan-neuronal *Rest* KO during postnatal development on the intrinsic excitability of excitatory pyramidal neurons in layer II/III of V1 were analyzed by patch-clamp recordings in acute cortical slices from the V1 cortex 4 weeks after transduction. We firstly examined the passive membrane properties and found that membrane capacitance, and resting membrane potential did not

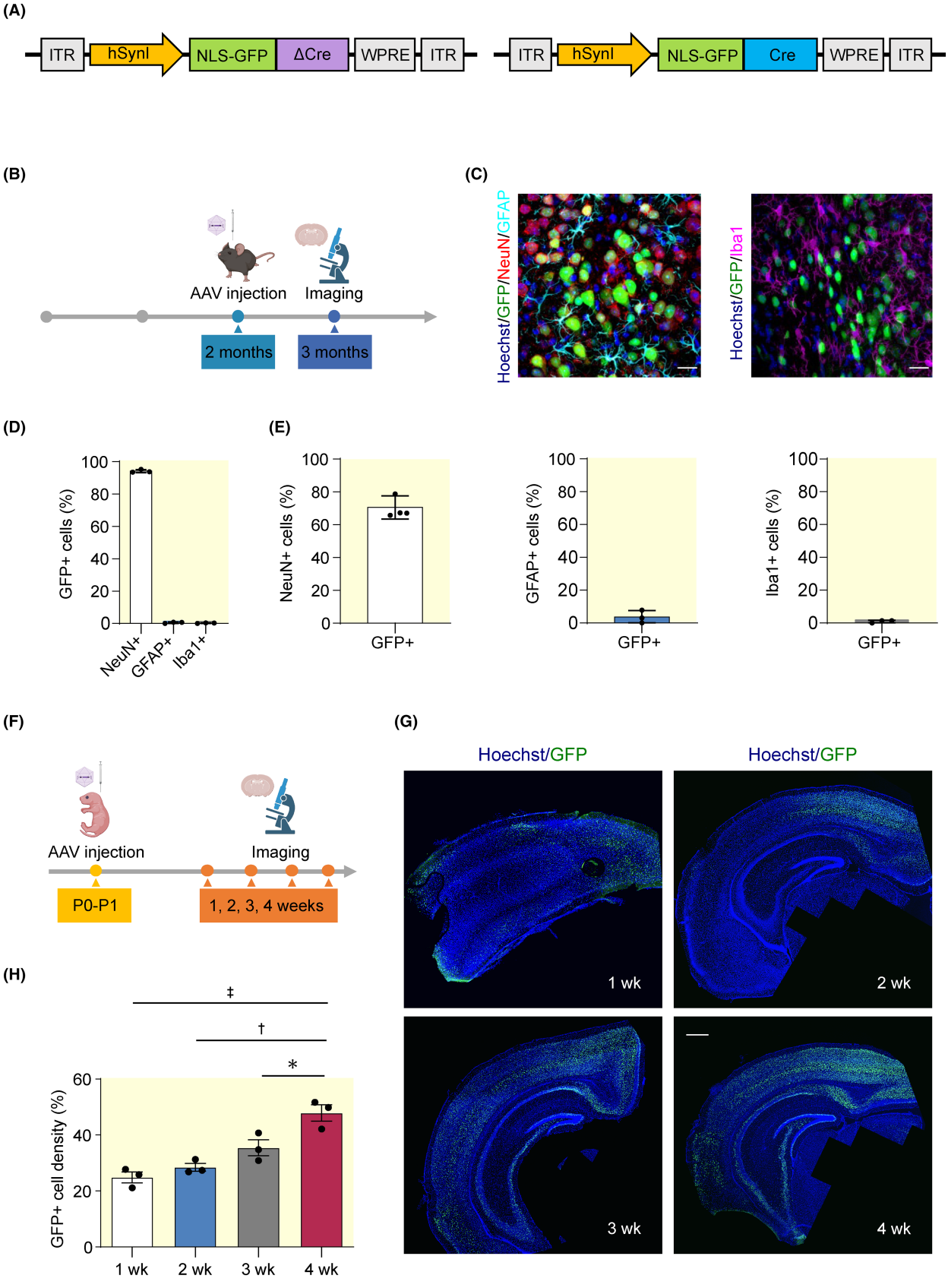

differ between ΔCre and Cre neurons (Figure S1). Upon steps of depolarizing injected current of increasing amplitude, the number of triggered action potentials (APs) was significantly higher in Cre-expressing pyramidal neurons compared to ΔCre controls (Figure 2A). The increased intrinsic excitability was witnessed by a significantly

FIGURE 1 Characterization of the pan-neuronal conditional *Rest*-KO. (A) Scheme of the AAV constructs used in the study. ITR, inverted terminal repeats; *hSyn1*, minimal promoter of human *SYN1*; NLS-GFP, nuclear localized green fluorescent protein; ΔCre, inactive Cre recombinase; Cre, active Cre recombinase; WPRE, woodchuck hepatitis virus post-transcriptional regulatory element. (B) Protocol of the imaging experiments used to characterize *hSyn1*-driven NLS-GFP expression. (C) Representative images of brain cortical slices from mice intracortically injected with AAV1/2 hSyn1-NLSx2-GFP stained for *left*: Hoechst (blue), anti-GFP (green), anti-NeuN (red), and anti-GFAP (cyan); *right*: Hoechst (blue), anti-GFP (green), and anti-Iba1 (magenta). Scale bars, 20 μm. (D) The *hSyn1* promoter-driven expression specificity was quantified as the ratio between the number of $NeuN^+/GFP^+$, $GFAP^+/GFP^+$ or $IBA1^+/GFP^+$ cells and the total number of GFP^+ cells. (E) Promoter penetrance expressed as the ratio of the number of GFP^+ cells over the total number of $NeuN^+$ (*left*), $GFAP^+$ (*middle*), and $Iba1^+$ (*right*) cells. (F) Protocol of the imaging experiments used to characterize the time-course of GFP expression. (G) Representative images of sagittal brain slices from pups injected in the lateral ventricles with 2 μL of PHP.eB hSyn1-NLS-GFP-ΔCre and sacrificed 1, 2, 3, and 4 weeks after the injections. Slices were stained for Hoechst (blue) and anti-GFP (green). Scale bar, 200 μm. (H) Time-course of GFP transduction expressed as percent density of GFP^+ cells. All data are expressed as means ± SEM with superimposed individual experimental points ($n = 3$ mice, 5 slices per mouse). $^*p < 0.05$, $^\dagger p < 0.01$, $^\ddagger p < 0.001$; one-way ANOVA/Tukey's tests.

lower rheobase and higher input resistance (Figure 2C). The waveform of the first evoked AP was studied using the phase-plane plot analysis, reporting the time derivative of membrane potential (dV/dt) versus the membrane voltage (Figure 2D). This analysis allows to extract the AP threshold (V_{thres}), AP peak (V_{max}), depolarizing, and repolarizing slopes, trough, and width.

All these waveform parameters were not significantly different between ΔCre and Cre neurons (Figure 2E–J). These data indicate that the absence of REST increases the intrinsic excitability of pyramidal neurons, consistent with its inhibitory role on the expression of voltage-dependent sodium channels $Na_V1.2$.[11,26]

3.3 | *Rest*-KO pyramidal neurons in layers II/III of the V1 cortex display an increased frequency of spontaneous and miniature excitatory postsynaptic currents

To study whether *Rest* deletion alter glutamatergic transmission, we recorded excitatory (Figure 3) and inhibitory (Figure 4) postsynaptic currents (EPSCs and IPSCs, respectively) from V1 pyramidal neurons of layers II/III after the postnatal deletion of REST. In spontaneous EPSC (sEPSCs) recordings (Figure 3A), we observed a significant increase in the mean event frequency in Cre-expressing neurons compared with ΔCre controls (Figure 3B, *left*), that was clearly apparent from the cumulative frequency distribution of the inter-event intervals (Figure 3B, *right*), while no changes were detected in the sEPSC amplitude (Figure 3C). As an increase in sEPSC frequency is attributable either to changes in spontaneous firing or to variation in the density and/or probability of spontaneous release of synaptic vesicles, we pharmacologically isolated AP-independent miniature PSCs (mEPSCs) by repeating the recordings in the presence of TTX (Figure 3D). We observed closely similar effects as for spontaneous currents: The frequency of mEPSCs in Cre neurons was significantly increased (Figure 3D, *left*), with a corresponding higher occurrence of shorter inter-event intervals, as compared with recording performed in ΔCre controls (Figure 3D, *right*), while no differences were found in the amplitude of mEPSCs (Figure 3F). While variations in mPSC amplitude are primarily related to the extent of response of postsynaptic receptors,[27] alterations in the frequency of mPSCs are commonly considered as related to the density of active synapses impinging on the patched neuron and/or to the probability of quantal neurotransmitter release.[28] Hence, our observations of a similar and selective higher frequency in Cre neurons for both sEPSCs and mEPSCs may suggest a higher number of excitatory synapses contacting principal neurons with the postnatal deletion of REST. The similar frequency changes observed in mEPSCs (stochastic release of single neurotransmitter quanta) and sEPSCs (which also include evoked neurotransmitter release induced by spontaneous action potentials) argue against a marked effect of the genotype on spontaneous firing activity.

To obtain further information on the excitation/inhibition balance (E/I) on layer II/III V1 pyramidal neurons, we next analyzed the frequency and amplitude of spontaneous (sIPSCs; Figure 4A) and miniature (mIPSCs; Figure 4D) inhibitory currents and found no significant differences in either frequency or amplitude of both sIPSCs (Figure 4B,C) and mIPSCs (Figure 4E,F) between Cre- and ΔCre-expressing neurons.

To uncover potential effects on quantal neurotransmitter release mechanisms, we also investigated whether REST deletion affected the kinetics of spontaneous and miniature EPSCs (Figure S2) and IPSCs (Figure S3). However, the analysis of the decay time, rise time and half-width showed no significant differences between ΔCre- and Cre-transduced neurons, making unlikely an effect of REST deletion on the kinetics of release.

When the E/I balance was determined in Cre- and ΔCre-expressing neurons by calculating the ratio between the mEPSC and mIPSC frequencies, it resulted

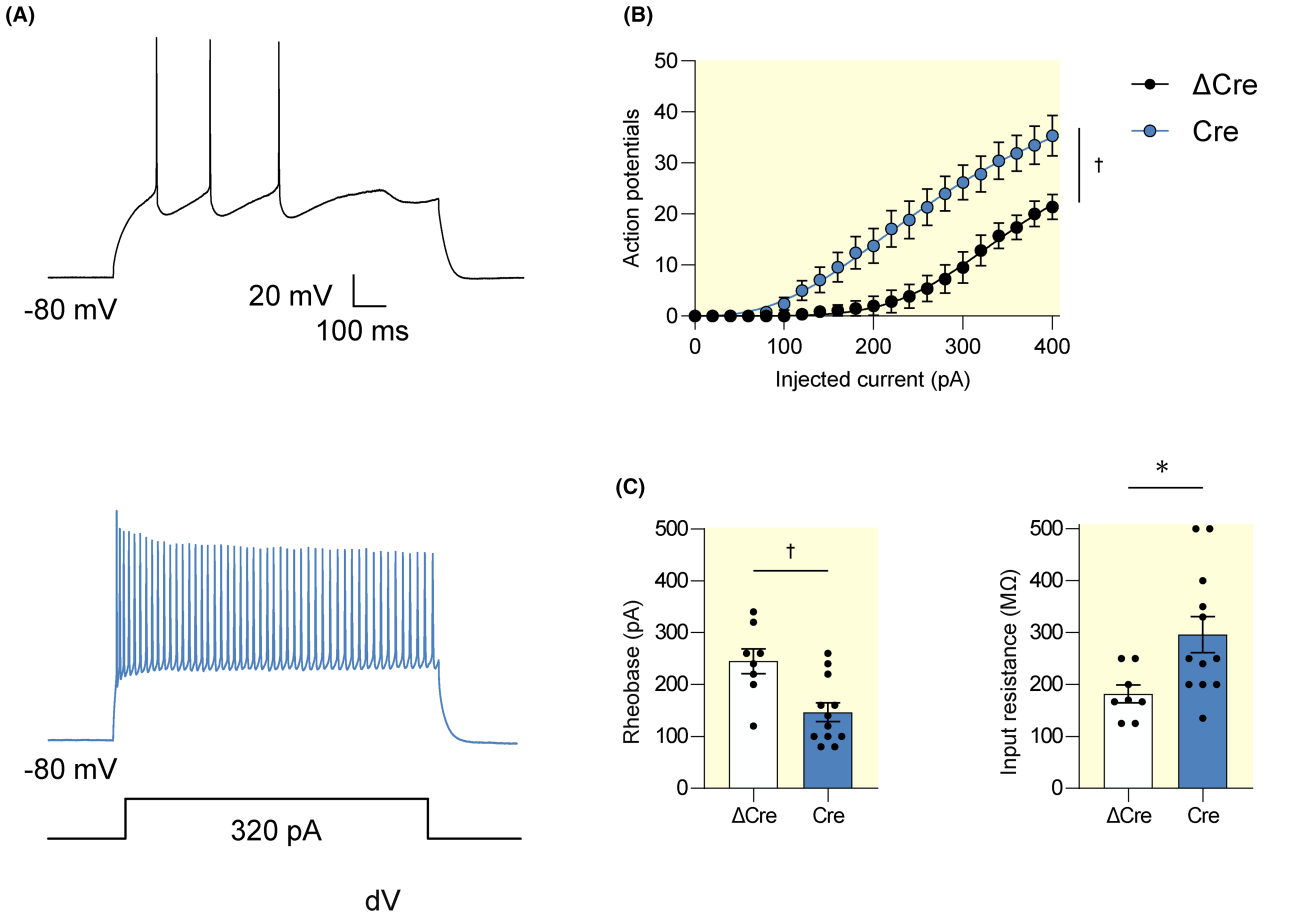

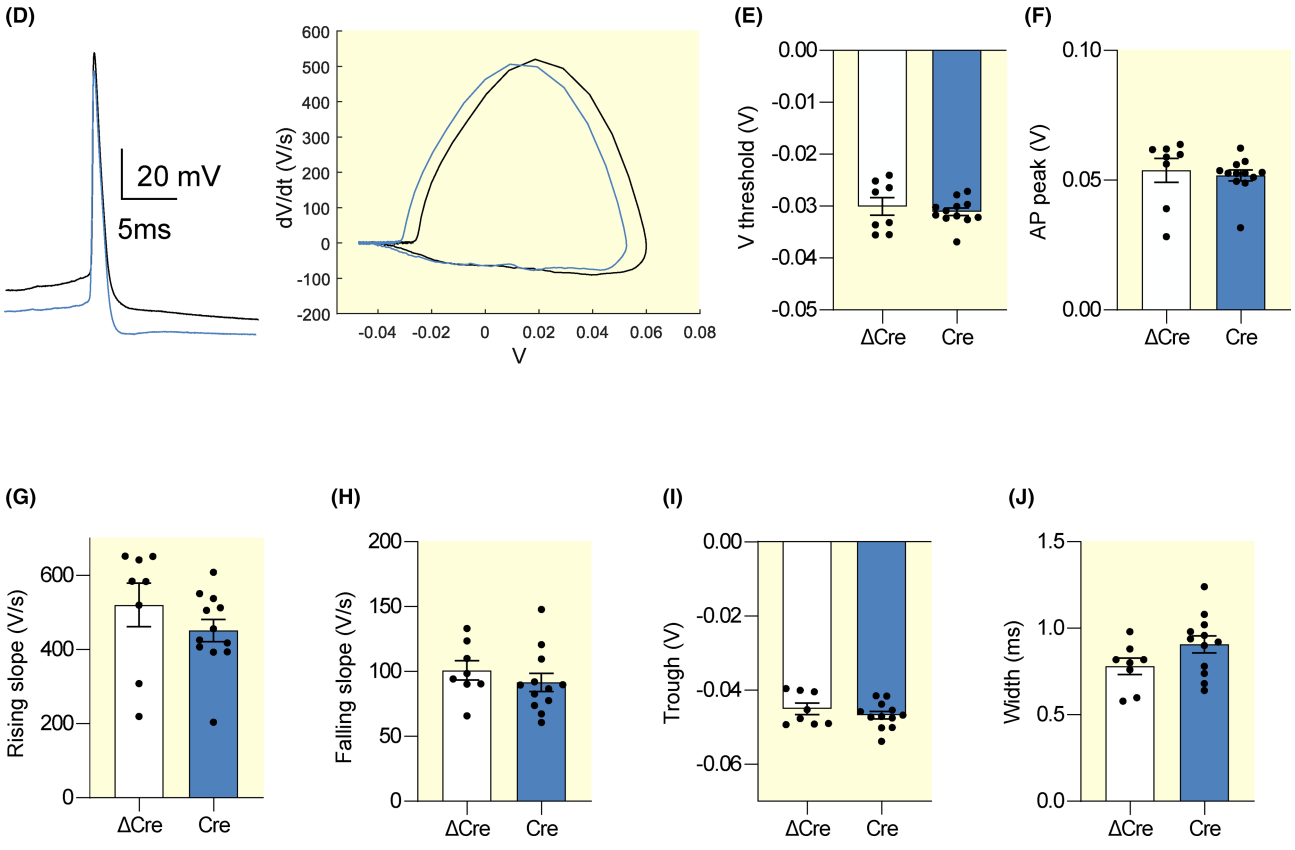

significantly increased under conditions of *Rest* deletion (Figure S4).

3.4 | Neuron-specific *Rest* KO in the V1 cortex is associated with a higher density of excitatory synapses

To better interpret the above-reported electrophysiological results, we analyzed the distribution of excitatory and inhibitory synapses in the V1 cortex of mice which had been transduced with either ΔCre or Cre for 4 weeks. To unambiguously identify excitatory synapses, we used the combination of the presynaptic marker VGLUT1 and the postsynaptic density marker PSD-95 (Figure 5A), while the identification of inhibitory synapses relied on the co-staining with the presynaptic marker VGAT and the postsynaptic scaffold protein Gephyrin (Figure 5B). We found a higher density of excitatory synapses in the V1 cortex from Cre-expressing mice as compared to ΔCre controls (Figure 5C, left panel; ΔCre: $1.82 \pm 0.15 \times 10^7/mm^3$; Cre: $3.13 \pm 0.52 \times 10^7/mm^3$; means ± SEM; $p = 0.03$). On the other hand, the density of inhibitory synapses in the very same area did not undergo detectable changes following *Rest* deletion compared with ΔCre controls (Figure 5C, right panel; ΔCre: $3.74 \pm 0.45 \times 10^7/mm^3$; Cre: $4.21 \pm 0.35 \times 10^7/mm^3$). The data confirm that the higher frequency of mEPSCs is attributable to an absolute increase in excitatory synaptic connections following postnatal deletion of *Rest*, while *Rest*-KO does not affect the development of inhibitory synaptic connections. Moreover, the absence of changes in mEPSC amplitude is consistent with previous results showing that the transcriptional effects of REST on synaptic transmission predominantly occur at the presynaptic level.[12] Altogether these results show that in normal conditions in V1 in vivo, REST negatively controls the number of active synaptic terminals of excitatory neurons (but not of inhibitory neurons) and the intrinsic excitability of layers II/III, consistent with its homeostatic control of network activity shown in cultured neurons.[11,12]

3.5 | Deletion of Rest early in development attenuates the seizure severity in response to repeated administration of the convulsant pentylenetetrazole

REST has been shown to play different roles under physiological conditions or under conditions of pathological hyperexcitability, ranging from homeostatic to pro-epileptogenic effects.[13,14,26,29,30] However, a clear picture is still largely missing.[29] To further elucidate the effects of the postnatal deletion of REST in neurons, we systemically administered the convulsant pentylenetetrazole (PTZ), known to alter network stability and homeostasis and simulate an epileptic-like condition by acting as a non-competitive antagonist of $GABA_A$ receptors.[31,32] $Rest^{GTi}$ mice were injected at P0/P1 with the AAV vectors expressing ΔCre (PHP.eB hSyn1-NLS-GFP-ΔCre) or Cre (PHP.eB hSyn1-NLS-GFP-Cre) in neurons and were treated, 1 month later, with two injections of a threshold dose (60 mg/kg) of PTZ administered at a 48-h interval or with vehicle to allow for the occurrence of transcriptional responses triggered by the first critical event (Figure 6A). Seizures were scored as previously described[21] from the least severe immobility (score 1) to the most severe tonic–clonic seizures (score 4/5) up to the possible death (score 6). Figure 6B displays the relative frequency distribution of scores in ΔCre- and Cre-transduced mice on the 2 days of PTZ administration, while the occurrence of stage 1, stage 4/5 and death is reported in Figure 6C–E. The seizure responses to the first PTZ dose (Day 1) in terms of score 1 and score 6 (death) were significantly more severe in *Rest*-deleted mice than in ΔCre-transduced controls, consistent with a homeostatic role of REST present in control mice under basal conditions. However, when the PTZ challenge was repeated 48 h later (Day 2), a significant decrease of the most severe events (score 4/5 and death) was observed in *Rest*-deleted mice, with a compensatory increase of the mildest score 1 seizures (Figure 6C–E). The shift from severe to mild seizure events in the absence of REST on the second convulsant challenge indicates that

FIGURE 2 Knockout of *Rest* in excitatory pyramidal neurons increases intrinsic excitability and action potential firing without altering the properties of the single action potential. Patch-clamp recordings were performed in acute neocortical slices from $Rest^{GTi}$ mice that had been transduced at P0/P1 with AAV-PHP.eB hSyn1-NLS-GFP viruses expressing either Cre or ΔCre, used as control. (A) Representative traces showing action potentials elicited by the same injected current (320 pA) in layer II/III pyramidal neurons in the V1 cortex from ΔCre- (*top*) and Cre- (*bottom*) transduced mice. (B) Plot of the number of elicited action potentials versus injected current in ΔCre- (red symbols) and Cre- (blue symbols) transduced mice. Points in the plot (means ± SEM) were fitted according to a logistic function. $^{\dagger}p < 0.01$ for genotype effect; two-way repeated measures ANOVA. (C) Bar plots showing the rheobase (*left*) and input resistance (*right*). $^{*}p < 0.05$, $^{\dagger}p < 0.01$; two-tailed unpaired Student's *t*-test. (D) Waveforms of representative action potentials (*left*) and the corresponding phase-plane plot analysis (*right*) elicited in ΔCre- (red) and Cre- (blue) transduced mice. (E–K) Properties of the single action potential extracted from the phase-plane plot analysis: V threshold (E), AP peak (F), rising slope (G), falling slope (H), trough (I), and width (J). Bar plots represent the means ± SEM with superimposed individual experimental points (ΔCre $n = 8$, Cre $n = 12$).

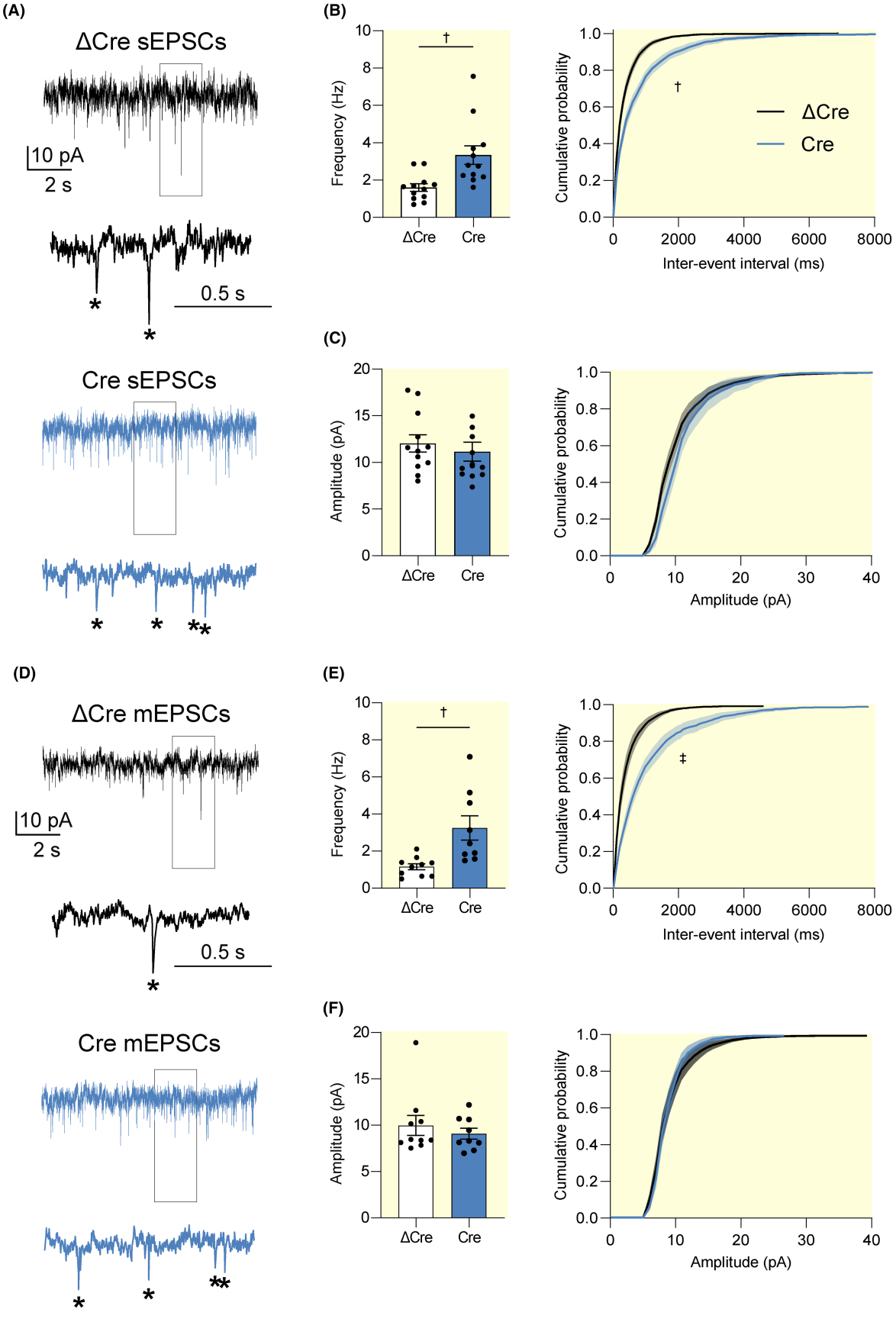

FIGURE 3 *Rest* knockout increases the frequency of spontaneous and miniature EPSCs without affecting spontaneous IPSCs. Patch-clamp recordings of sEPSCs and mEPSCs in layer II/III pyramidal neurons of the V1 cortex from acute brain slices from P30-40 $Rest^{GTi}$ mice that had been transduced at P0/P1 with AAV-PHP.eB hSyn1-NLS-GFP viruses expressing either Cre or ΔCre recombinase. (A) Representative traces of sEPSCs recorded in ΔCre- (red) and Cre- (blue) transduced mice. The bottom panels represent the boxed traces in an expanded temporal scale (events marked with asterisks). plotted in two temporal scales. (B) Bar plots of sEPSC frequency (*left*) and cumulative probability of the inter-event intervals (*right*). (C) Bar plots of sEPSC amplitude (*left*) and cumulative probability of the amplitude (*right*). (D) Representative traces of mEPSCs recorded in ΔCre- (red) and Cre- (blue) transduced mice. The bottom panels represent the boxed traces in an expanded temporal scale (events marked with asterisks). (E) Bar plots of mEPSC frequency (*left*) and cumulative probability of the inter-event intervals (*right*). (F) Bar plots of mEPSC amplitude (*left*) and cumulative probability of the amplitude (*right*). Data in bar plots are means ± SEM with superimposed individual experimental points (sEPSCs: $n = 12$ for both ΔCre and Cre; mEPSCs: $n = 12$ for both ΔCre and Cre). $^{\dagger}p < 0.01$; two-tailed unpaired Student's *t*-test (bar plots); $^{\dagger}p < 0.01$, $^{\ddagger}p < 0.001$; Kolmogorov–Smirnov's test (cumulative curves). Scale bars, 20 pA and 2 s.

under pro-epileptic condition, the presence of REST may switch from homeostatic to pro-epileptogenic.

3.6 | *Rest* deletion loses its homeostatic role under pro-epileptic conditions

To investigate at the cellular level the effects of *Rest* deletion under this induced ictogenic condition, we performed patch-clamp recordings on acute V1 cortical slices obtained 30 min after the second PTZ injection. We first measured the passive membrane properties and found that membrane capacitance, and resting membrane potential were similar between ΔCre and Cre neurons (Figure S5). Upon steps of depolarizing injected current of increasing amplitude, the number of triggered action potentials (APs) was significantly higher in Cre-expressing pyramidal neurons compared with ΔCre controls, as previously found under basal conditions (Figure S6A). However, under ictogenic conditions, the increased intrinsic excitability of Cre-transduced mice was less pronounced than that observed under basal conditions, with a trend toward significance for the rheobase ($p = 0.054$) and no significant changes in input resistance and AP waveform parameters (threshold, peak, depolarizing, and repolarizing slopes, trough, and width of the AP waveform) (Figure S6B–I).

Next, we investigated whether the changes in glutamatergic and GABAergic transmission caused *Rest* deletion were affected under the pro-epileptic conditions. Cre mice treated with two vehicle administrations confirmed the selective increase of sEPSC (Figure 7A,B) and mEPSC (Figure 7C,D) frequency with respect to ΔCre controls. However, when both experimental groups were challenged with the tandem PTZ dose, Cre mice displayed an increase in sEPSC frequency but were unable to increase the mEPSC frequency, while ΔCre controls showed robust increases in the frequency of both sEPSCs and mEPSCs (Figure 7B,D). No differences in both sEPSC and mEPSC amplitudes were observed across all experimental groups, confirming the presynaptic origin of the described effects (Figure 7B,D). In Cre mice treated with PTZ, two-way ANOVA analysis of mEPSC frequency showed a significant interaction between treatment and genotype (p value = 0.0137). These data show that neuron-specific loss of REST increases the frequency of both sEPSCs and mEPSCs and that, unlike in control ΔCre mice, a further increase in mEPSC frequency appears to be saturated, since the instauration of a hyperexcitability condition by PTZ does not trigger any further effect. Therefore, the absence of REST under ictogenic conditions seems to dampen, rather than increase hyperexcitability.

The same experimental paradigm was used to study sIPSCs and mIPSCs (Figure 8). Consistent with previous results, we did not observe any difference in the frequency and amplitude of sIPSCs before and after the PTZ challenge in both ΔCre and Cre mice (Figure 8A,B). Conversely, Cre mice experienced a decrease in the frequency mIPSCs after the PTZ challenge, while this parameter was not affected in ΔCre mice (Figure 8C,D). Two-way ANOVA analysis of mIPSC frequency in Cre mice treated with PTZ, showed a significant interaction between treatment and genotype (p value = 0.0252). No differences in both sIPSC and mIPSC amplitudes were observed across all experimental groups (Figure 8B,D). Such decrease in mIPSC frequency observed in REST-deleted mice under pro-epileptic conditions could be secondary to the failure of PTZ to increase the excitatory input to pyramidal neurons and is consistent with the described role of REST in promoting an activity-dependent inhibitory-onto-excitatory synaptogenesis.[13]

Interestingly, the E/I balance, determined by calculating the ratio between the mEPSC and mIPSC frequencies in Cre- and ΔCre-expressing neurons after the second PTZ dose, was not significantly changed between the two genotypes (Figure S7).

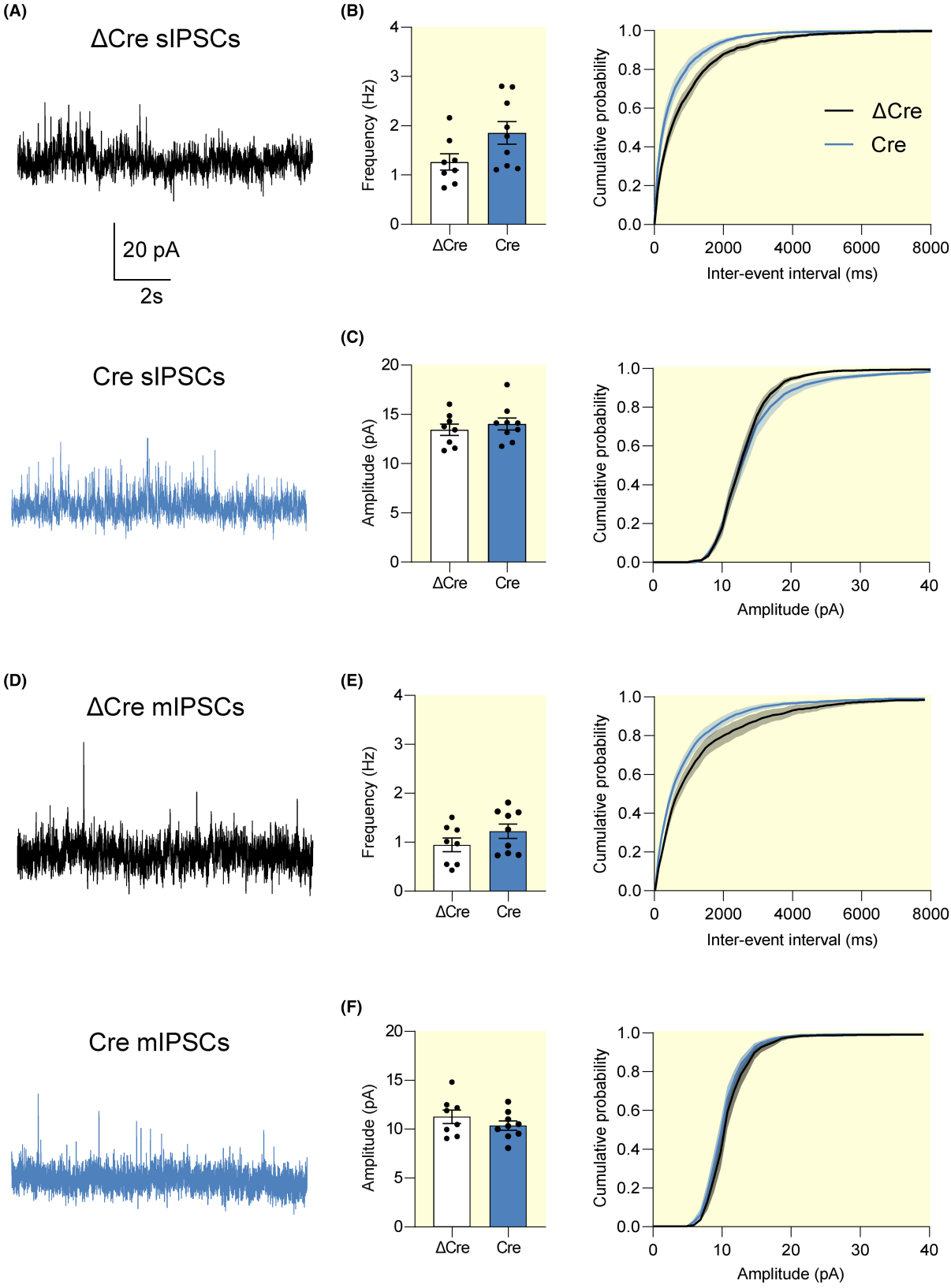

4 | CONCLUSION

An abnormal, recurrent hyperactivity is a distinctive trait of a brain affected by epilepsy.[33,34] While mechanisms of homeostatic plasticity dampen hyperactivity act under physiological conditions,[35] there is evidence that they cannot counteract the abnormal network activity during epilepsy.[30] The inability of homeostatic plasticity to control network hyperexcitability might be linked to deficiencies in cellular and/or molecular

FIGURE 4 *Rest* knockout does not affect the frequency and amplitude of spontaneous and miniature IPSCs. Patch-clamp recordings of sIPSCs and mIPSCs in layer II/III pyramidal neurons of the V1 cortex from acute brain slices from P30-40 $Rest^{GTi}$ mice that had been transduced at P0/P1 with AAV-PHP.eB hSyn1-NLS-GFP viruses expressing either Cre or ΔCre recombinase. (A) Representative traces of sIPSCs recorded in ΔCre- (red) and Cre- (blue) transduced mice. (B) Bar plots of sIPSC frequency (*left*) and cumulative probability of the inter-event intervals (*right*). (C) Bar plots of sIPSC amplitude (*left*) and cumulative probability of the amplitude (*right*). (D) Representative traces of mIPSCs recorded in ΔCre- (red) and Cre- (blue) transduced mice. (E) Bar plots of mIPSC frequency (*left*) and cumulative probability of the inter-event intervals (*right*). (F) Bar plots of mIPSC amplitude (*left*) and cumulative probability of the amplitude (*right*). Data in bar plots are means ± SEM with superimposed individual experimental points (sIPSCs: $n = 8$ and $n = 9$ for ΔCre and Cre, respectively; mIPSCs: $n = 8$ and $n = 9$ for ΔCre and Cre, respectively). $p > 0.05$; two-tailed unpaired Student's *t*-test (bar plots); $p > 0.05$; Kolmogorov–Smirnov's test (cumulative curves). Scale bars, 20 pA and 2 s.

mechanisms and/or to the establishment of pathological long-term plasticity phenomena and could, in principle, be counteracted by an activity-dependent exogenous potentiation of homeostatic mechanisms.[36,37] At the transcriptomic level, differential changes in the regulation of gene expression could affect homeostatic plasticity during long-lasting epileptic states. Accumulating evidence indicates that identical transcriptomic pathways associated with homeostasis, which under certain circumstances support the restoration of a normal physiological balance, can have paradoxical effects under pathologic conditions intensifying, rather than counteracting, neuronal hyperactivity.[38] One transcription factor that has been described to have such a dual role is REST. While it is widely accepted that REST is induced in an activity-dependent fashion in neurons and participates in homeostatic plasticity mechanisms, it is still largely debated whether REST has a pro- or anti-epileptic function under pathological hyperactivity conditions.[30,36]

Homeostatic plasticity undergoes regulation throughout development, and the nature of the compensation is contingent upon the state of the network, rather than being predetermined at the individual cell level.[39] It is known that REST is not only critical for neuronal differentiation but is also involved in the fine-tuning of the network connectivity and plasticity during the postnatal critical period.[4] Here, we addressed the role of the widespread pan-neuronal knockout of REST induced at birth in a REST-cKO mouse on the functional and morphological maturation of synaptic connectivity in the V1 cortex and what consequences REST deletion may have on seizures susceptibility using the recurrent acute seizure model of tandem PTZ administration. The seizure provocation model using PTZ is widely used to assess seizure propensity and for its actions related to "kindling."[21,40] PTZ is a convulsant that inhibits GABAergic neurotransmission by being a non-competitive antagonist of $GABA_A$ receptors, similarly to picrotoxin, even if the precise mechanism of action is not completely clear.[31,32]

To avoid the discrepancies existing in the literature dealing with *Rest*-cKO mice in which residual *Rest* transcription is present,[41,42] we used a recently generated *Rest*-cKO mouse, $Rest^{GTi}$, in which no expression of full length or truncated variants of REST occurs.[16] In this strain, we generated a widespread neuron-specific *Rest*-KO by bilaterally injecting in the lateral ventricles of newborn mice an engineered PHP.eB AAV vector with increased diffusibility across biological barriers encoding CRE recombinase under the control of the minimal *hSyn1* promoter. To create a recurrent acute seizure model, we used a tandem administration of two PTZ doses at a 2 days-interval with the aim to induce a hyperactivity state that, in wild-type animals, induces REST transcription and activity.[11–13]

We have found that the early postnatal *Rest* deletion causes an increased excitability of cortical pyramidal neurons associated with strengthening of the excitatory synaptic connectivity, while the density and functionality of inhibitory synapses onto pyramidal neurons are not affected. Thus, the absence of REST in the critical postnatal period of synapse development and rearrangement brings about an E/I imbalance at the level of cortical neurons, at least of layer II/III pyramidal neurons of the primary visual cortex. While the increased excitability is consistent with the repression of the expression of voltage-dependent sodium channels, such as *Scn2a*, by REST,[11,26] the change in the E/I synaptic balance is specific for excitatory synaptic and is obtained at the presynaptic level as consequence of an increased density of excitatory connections. These results are consistent with previous work showing that the hyperactivity-dependent induction of REST by 4-aminopyridine reduced the strength of excitatory synapses in primary hippocampal neurons by acting at the presynaptic level.[12] These data therefore indicate that, under physiological conditions, REST negatively controls the intrinsic excitability and synaptic excitatory inputs to cortical pyramidal neurons.

However, when a recurrent epileptic condition was reproduced by the tandem administration of PTZ, *Rest*-KO mice were unable to increase the frequency of mEPSCs as control animals did, suggesting that the excitatory synapses hyperconnected network developed postnatally was saturated or refractory to a further increase in excitatory strength induced by epileptogenic stimuli. The lack of

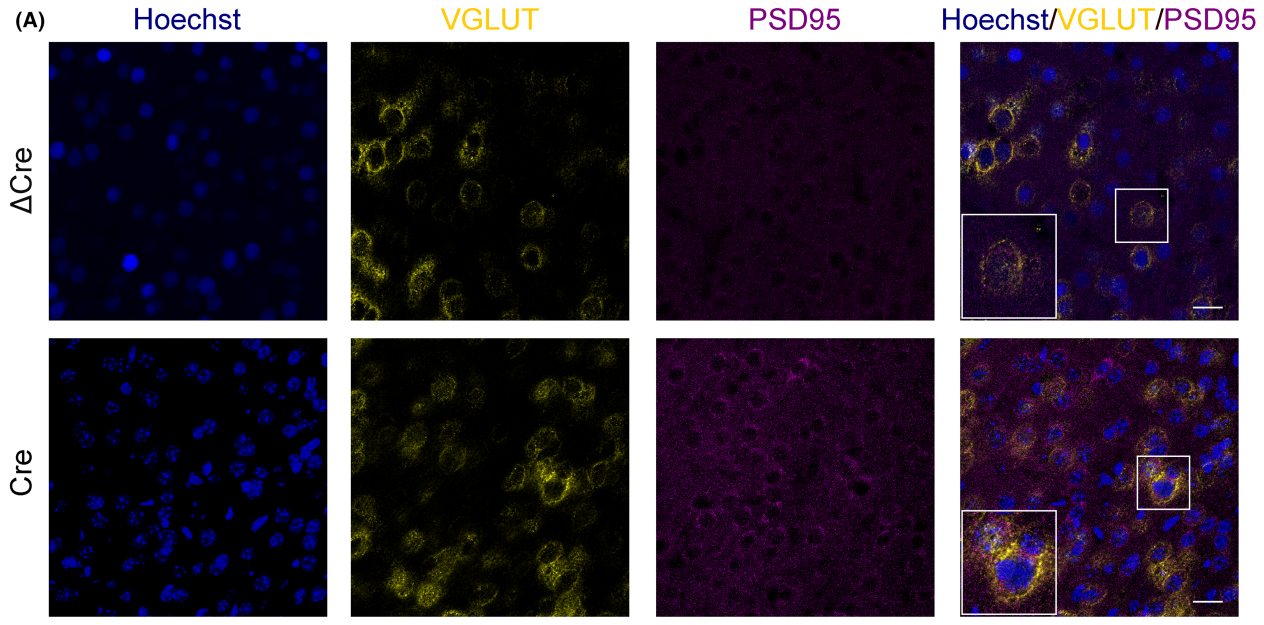

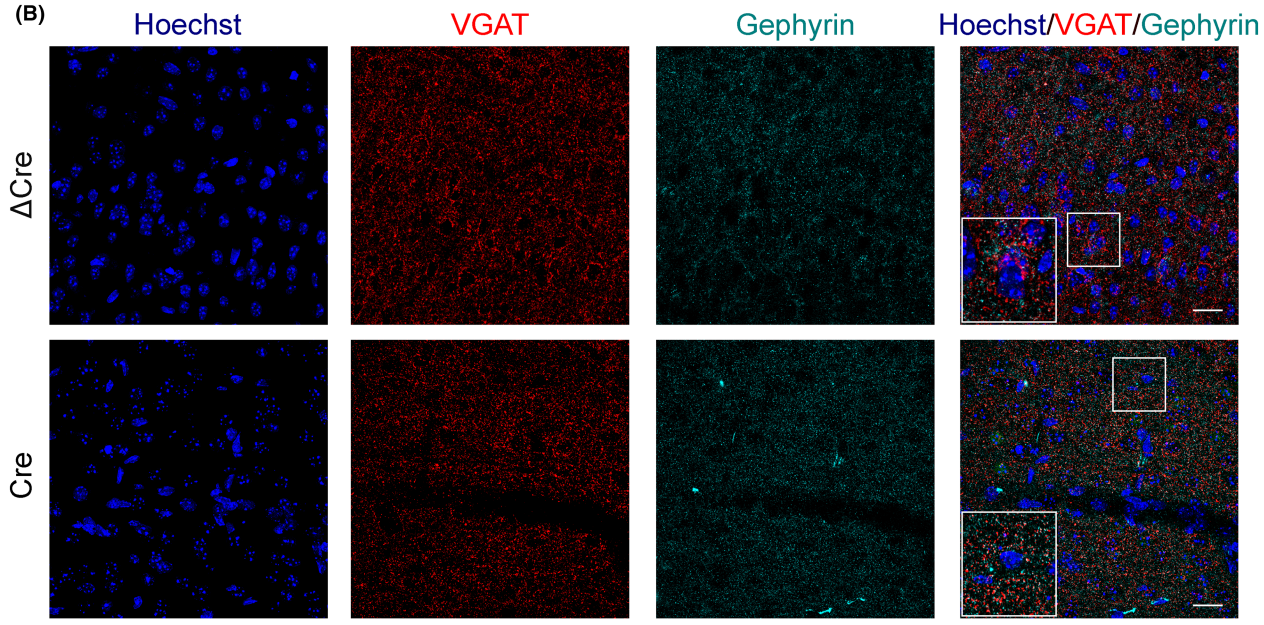

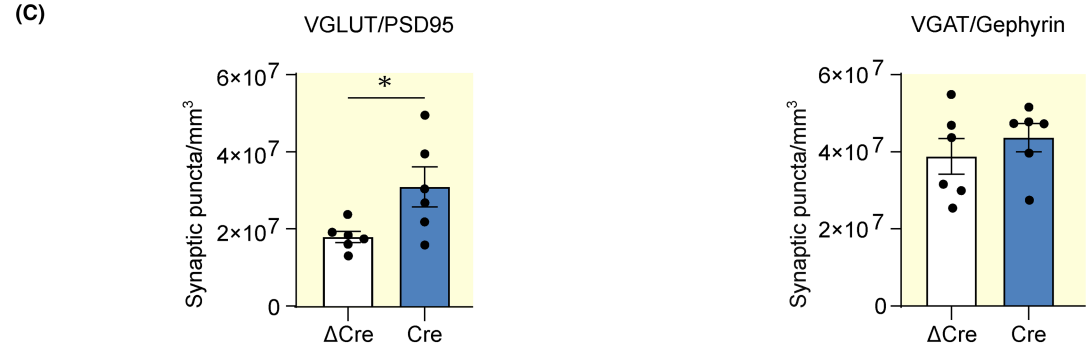

FIGURE 5 *Rest* knockout increases the density of excitatory, but not inhibitory, synapses in the V1 cortex. (A, B) Representative images of brain cortical slices of the V1 cortex from *Rest*^{GTi} mice injected in the lateral ventricles at P0/P1 with 2 µL of either PHP.eB hSyn1-NLS-GFP-ΔCre or PHP.eB hSyn1-NLS-GFP-Cre. In (A) sections were stained with (from left to right): Hoechst (blue), anti-VGLUT (yellow), and anti-PSD-95 (magenta). In (B) sections were stained with (from left to right): Hoechst (blue), anti-VGAT (red), and anti-Gephyrin (cyan). The rightmost panel in (A) and (B) represents the merge of the three stainings with an inset at higher magnification (white square). Scale bars, 20 µm (10 µm in the insets). (C) Density of excitatory (*left*) and inhibitory (*right*) synapses (synaptic puncta/mm^3). Data are expressed as means ± SEM with superimposed individual experimental points. *$p < 0.05$; unpaired Student's *t*-test ($n = 6$ mice, 3 slices per mouse).

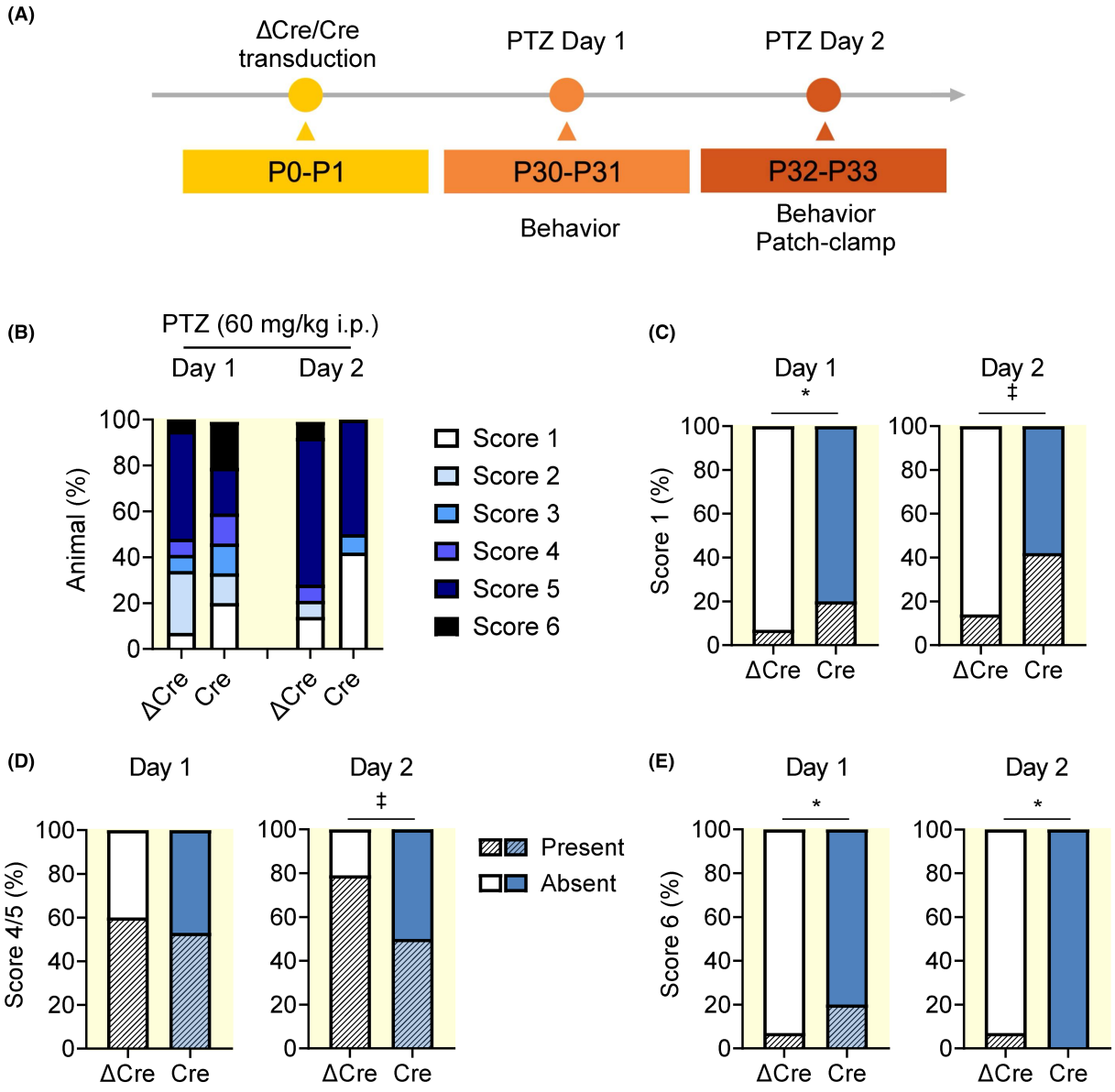

FIGURE 6 *Rest*-KO mice show less severe seizures and higher survival rate after a second dose of PTZ. (A) Timeline of the experimental procedure. *Rest*^{GTi} pups, injected at P0/P1 with AAV-PHP.eB hSyn1-NLS-EGFP viruses expressing either Cre or ΔCre, were given a first injection of PTZ (60 mg/kg) at P30/P31. Forty-eight hours later (P32/P33), mice were given a PTZ boost at the same dose and were sacrificed after 30 min. (B) Occurrence of the various seizure after the first (Day 1) and the second (Day2) PTZ dose (60 mg/kg, i.p.). The phenotype of the tested animals is represented according to the following color code: immobility (score 1, white), twitch (score 2, light blue), Straub's tail (score 3, cyan), mild seizure (score 4, blue), severe seizure (score 5, dark blue), and death (score 6, black). (C–E) Relative frequency of occurrence of the mildest score 1 (immobility; C), the most severe tonic–clonic seizures (score 4/5; D) and death (score 6; E) in the two experimental groups at Day 1 and Day 2. *$p < 0.05$, ‡$p < 0.001$; Fisher's exact test ($n = 10$ mice for both ΔCre- and Cre).

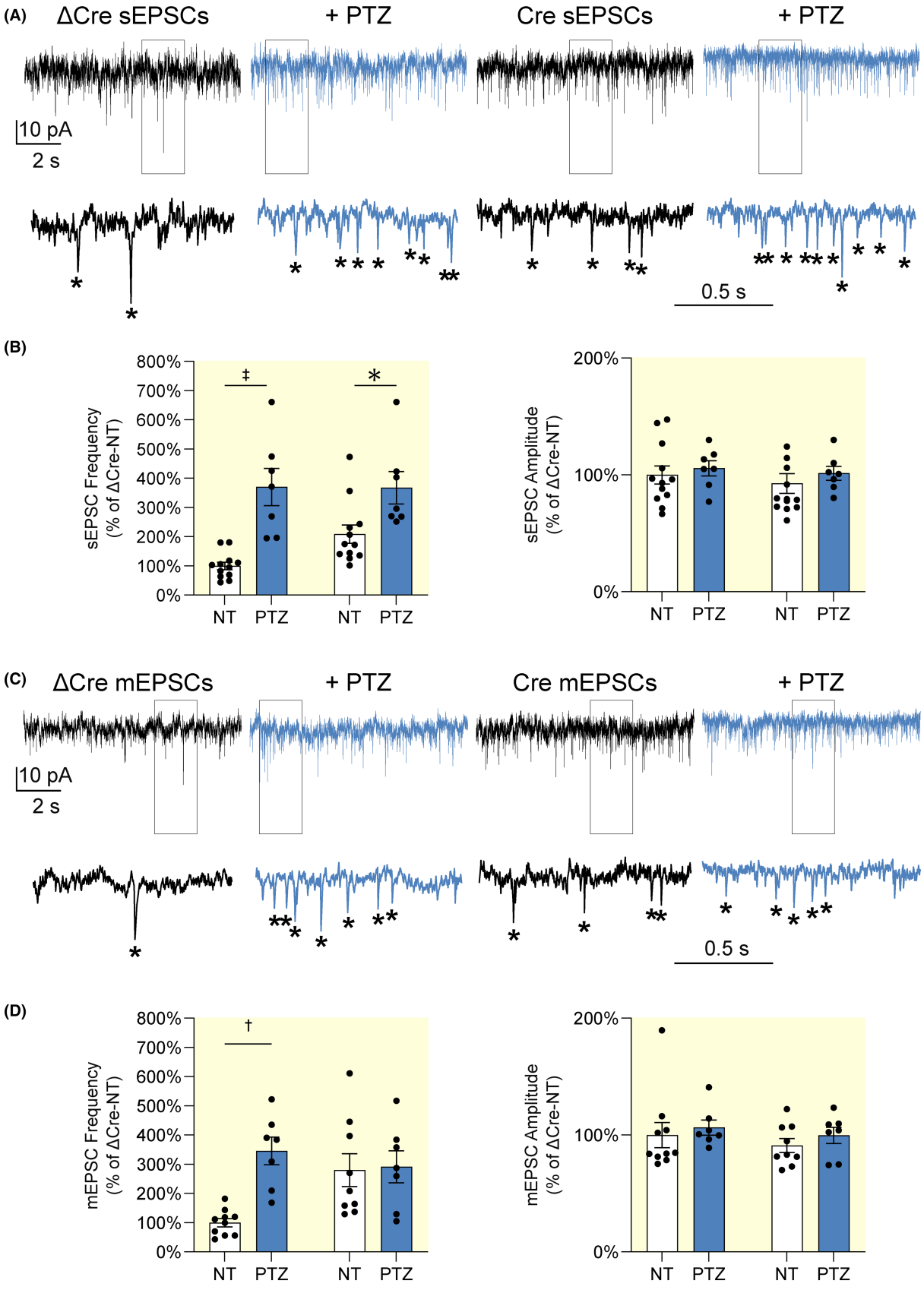

increase of excitatory strength induced by the convulsant was paralleled by the lower propensity to experience severe tonic–clonic seizures and death after the second PTZ challenge exhibited by *Rest*-KO mice, consistent with a pro-epileptogenic, rather than homeostatic, role of REST under epileptic-like conditions. The associated decrease

FIGURE 7 Treatment with PTZ does not increase the frequency of mEPSCs in *Rest* knockout mice. After the tandem PTZ challenge described in Figure 6A, mice were sacrificed, and the brain was extracted and sliced to perform whole-cell patch-clamp electrophysiology in layers II/III of the V1 cortex. (A) Representative traces of sEPSCs from ΔCre- and Cre-transduced mice that were either administered with vehicle (untreated) or treated with PTZ. The bottom panels represent the boxed traces in an expanded temporal scale (events marked with asterisks). (B) Bar plots of sEPSC frequency (*left*) and amplitude (*right*) recorded in untreated (NT) or PTZ-treated ΔCre- and Cre-transduced mice. (C) Representative traces of mEPSCs from ΔCre- and Cre-transduced mice that were either administered with vehicle (untreated) or treated with PTZ. The bottom panels represent the boxed traces in an expanded temporal scale (events marked with asterisks). (D) Bar plots of mEPSC frequency (*left*) and amplitude (*right*) recorded in untreated (NT) or PTZ-treated ΔCre- and Cre-transduced mice. Data in bar plots are means ± SEM with superimposed individual experimental points (sEPSCs: $n = 12$ for both NT Cre and ΔCre; $n = 7$ for both PTZ Cre and ΔCre. mEPSCs: $n = 10$ and $n = 7$ for NT ΔCre and Cre, respectively; $n = 7$ both PTZ Cre and ΔCre). *$p < 0.05$, †$p < 0.01$, ‡$p < 0.001$; two-way ANOVA/Tukey's tests.

in mIPSC frequency observed in REST-deleted mice subjected to pro-epileptic conditions is the only change that was detected in the inhibitory strength upon REST deletion and is likely secondary to the failure of PTZ to increase the excitatory input to pyramidal neurons or it may depend, at least in part, on the effects of PTZ that is known to non-competitively block $GABA_A$ receptors. On the other hand, the fact that REST acts on both neuronal populations is supported by the evidence that REST controls the expression of both excitatory and inhibitory genes[26] and promotes activity-dependent inhibitory-onto-excitatory synaptogenesis *in vitro*.[13] However, the failure to prevent the increase of sEPSCs in the network, and the lack of significant changes in sIPSC frequency after PTZ treatment suggest that the role of REST under pro-epileptic conditions is more complex, possibly involving, inter alia, alterations in the spontaneous firing activity of both excitatory and inhibitory neurons.

While the observed role played by REST during early development is consistent with its well-characterized homeostatic function on neuronal network activity, its role played during the epilepsy pathogenesis is still largely controversial. Conditional KO mice in which REST was deleted in CaMKII-expressing neurons had higher susceptibility to kindling, indicating an anti-epileptic role of REST in adult excitatory neurons.[41] On the other hand, cKO mice in which REST was deleted using the neuron-specific enolase promoter displayed a higher resistance to PTZ-induced tonic–clonic seizures with an increase of the PTZ lethal dose.[42] Consistently, a decrease in kainic acid-induced seizures was observed when REST activity was inhibited by the expression of an inhibitor of the REST cofactor mSin3.[26] Similar results were found by McClelland et al.[30] who reported that the increase of REST in response to kainic acid-induced epileptogenic insult contributes to epileptogenesis by repression of a group of genes that critically influence neuronal function, opening the possibility that the pattern of REST-repressed genes changes from physiological to pro-epileptic conditions. While these partially conflicting results can be explained by the different cKO strains, age, cell types, and temporal profile of REST deletion, our data with early postnatal pan-neuronal REST deletion are consistent with a switch in REST action between homeostatic to pro-epileptogenic under pathological hyperexcitability conditions. This possibility is also supported by a recent study showing that the conditional *Rest*-KO in adult forebrain excitatory neurons reduces seizure excitability to chemical PTZ kindling.[20] However, we cannot rule out the possibility that the precocious postnatal knockout of REST and the resulting hyperactivity of neuronal networks may trigger compensatory changes at the transcriptional and post-transcriptional levels that render the brain less vulnerable to epileptogenic insults.

It is possible that the controversial information present in the literature on the role of REST in epilepsy and homeostatic plasticity is related to the diversity of studied neuronal population (excitatory versus inhibitory) and of the cKO mouse strain used (complete vs. incomplete KO). Further studies are necessary to fully understand the environmental conditions under which REST acts as pro- or anti-epileptic transcriptional regulator. However, from previous reports and the current study, it emerges a picture in which REST counteracts increased excitability under physiological conditions by acting as a homeostatic regulator of neuronal activity, while it boosts hyperexcitability associated with epileptogenic neurons potentially supporting epileptogenesis. It is tempting to speculate that the switch from homeostatic to pro-epileptogenic REST activity occurs when the primary epileptogenic insult has triggered a sequence of heterostatic plasticity events that progressively and irreversibly remove the network activity level from the physiological range.

AUTHOR CONTRIBUTIONS

Fabio Benfenati: Funding acquisition; writing – original draft; writing – review and editing; resources; conceptualization; formal analysis; supervision; investigation. **Carmela Vitale:** Writing – original draft; methodology; validation; visualization; investigation;

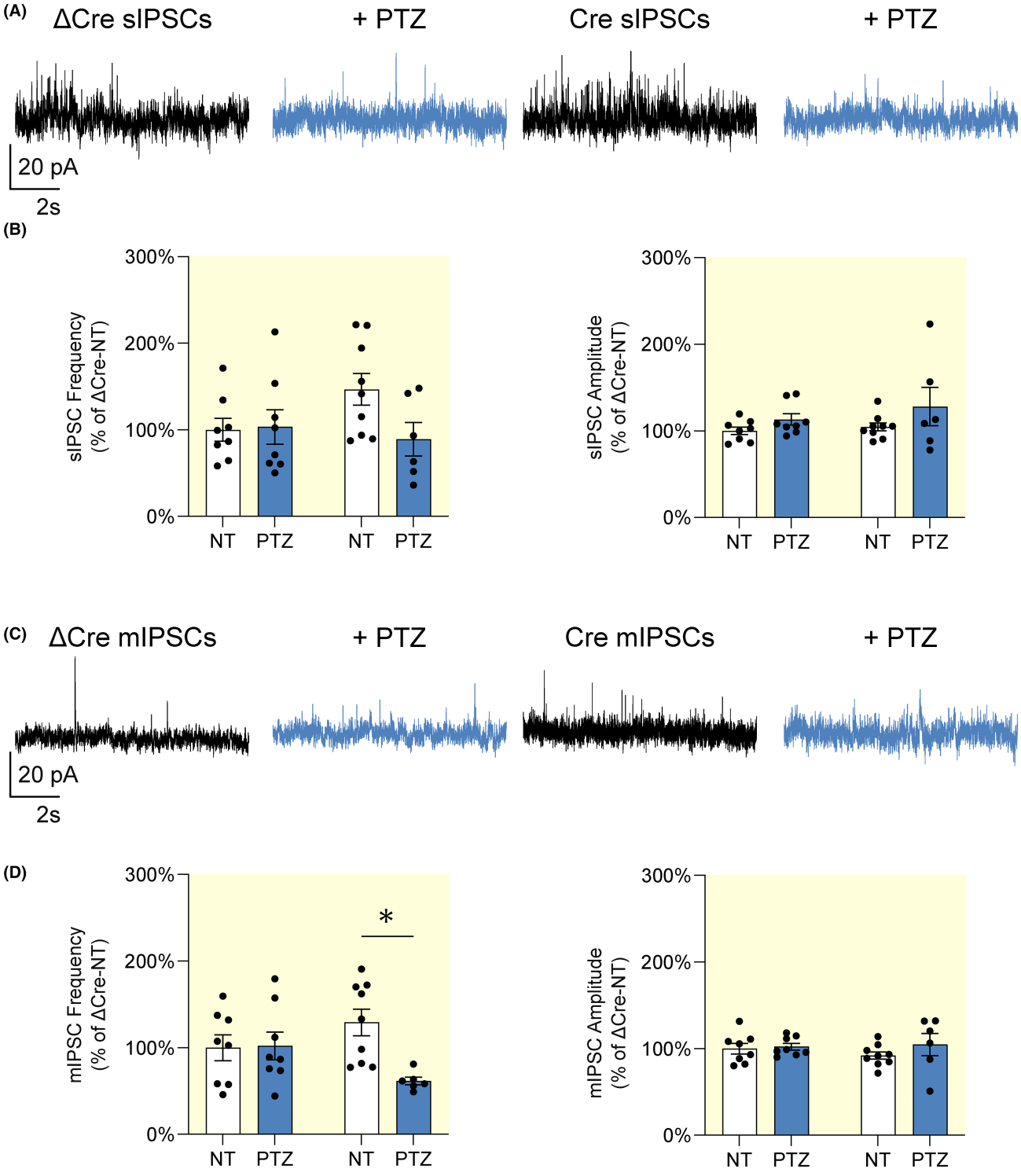

FIGURE 8 Treatment with PTZ decreases the frequency of mIPSCs in *Rest* knockout mice. After the tandem PTZ challenge described in Figure 6A, mice were sacrificed, and the brain was extracted and sliced to perform whole-cell patch-clamp electrophysiology in layers II/III of the V1 cortex. (A) Representative traces of sIPSCs from ΔCre- and Cre-transduced mice that were either administered with vehicle (untreated) or treated with PTZ. (B) Bar plots of sIPSC frequency (*left*) and amplitude (*right*) recorded in untreated (NT) or PTZ-treated ΔCre- and Cre-transduced mice. (C) Representative traces of miPSCs from ΔCre- and Cre-transduced mice that were either administered with vehicle (untreated) or treated with PTZ. (D) Bar plots of mIPSC frequency (*left*) and amplitude (*right*) recorded in untreated (NT) or PTZ-treated ΔCre- and Cre-transduced mice. Data in bar plots are means ± SEM with superimposed individual experimental points (sIPSCs and mIPSCs: $n = 8$ and $n = 9$ for NT ΔCre and Cre, respectively; $n = 8$ and $n = 6$ for PTZ ΔCre and Cre, respectively). *$p < 0.05$; two-way ANOVA/Tukey's tests. Scale bars, 20 pA and 2 s.

data curation. **Giulia Natali:** Writing – original draft; methodology; validation; visualization; investigation; data curation. **Maria Sabina Cerullo:** Writing – original draft; investigation; methodology; validation; visualization; data curation. **Thomas Floss:** Methodology; resources. **Caterina Michetti:** Methodology; supervision; investigation; writing – review and editing; data curation. **Giorgio Grasselli:** Supervision; data curation; formal analysis; visualization; writing – original draft; writing – review and editing; investigation.

ACKNOWLEDGMENTS

We are grateful to Gail Mandel (Vollum Institute, Portland, OR) and the German Gene Trap Consortium (GGTC-Partners) for providing us with the REST conditional knockout mice and Pietro Baldelli for useful suggestions and critical reading of the manuscript. We also thank drs. Riccardo Navone (Istituto Italiano di Tecnologia, Genova, Italy), Laura Emionite and Michele Cilli (IRCCS Ospedale Policlinico San Martino, Genova, Italy) for assistance in breeding the mice; drs. Diego Moruzzo and Arta Mehilli (Istituto Italiano di Tecnologia, Genova, Italy) for help in genotyping; drs. Ilaria Dallorto and Rossana Ciancio (Istituto Italiano di Tecnologia, Genova, Italy) for administrative assistance. Open access funding provided by BIBLIOSAN.

FUNDING INFORMATION

The study was supported by research grants from the Italian Ministry of Health (Ricerca Finalizzata Giovani Ricercatori GR-2019-12 370 176), Compagnia di San Paolo Torino (ID ROL34760 to FB), the Italian Ministry of University and Research (PRIN 2020-WMSNBL and PRIN 2022-XWEYBN to FB and PRIN2020 EU-NextGenEU PNRR PE0000006 Mnesys to GG), and by IRCCS Ospedale Policlinico San Martino (5x1000 and Ricerca Corrente).

CONFLICT OF INTEREST STATEMENT

The authors have no relevant financial or non-financial interests to disclose.

DATA AVAILABILITY STATEMENT

The data that support the findings of this study are available upon reasonable request to the corresponding authors.

ORCID

Giorgio Grasselli https://orcid.org/0000-0002-2942-9615
Fabio Benfenati https://orcid.org/0000-0002-0653-8368

REFERENCES

1. Ooi L, Wood IC. Chromatin crosstalk in development and disease: lessons from REST. *Nat Rev Genet*. 2007;8(7):544-554.
2. Bruce AW, Donaldson IJ, Wood IC, et al. Genome-wide analysis of repressor element 1 silencing transcription factor/neuron-restrictive silencing factor (REST/NRSF) target genes. *Proc Natl Acad Sci*. 2004;101(28):10458-10463.
3. Ballas N, Grunseich C, Lu DD, Speh JC, Mandel G. REST and its corepressors mediate plasticity of neuronal gene chromatin throughout neurogenesis. *Cell*. 2005;121(4):645-657.
4. Hwang J-Y, Zukin RS. REST, a master transcriptional regulator in neurodegenerative disease. *Curr Opin Neurobiol*. 2018;48:193-200.
5. Yeo M, Berglund K, Augustine G, Liedtke W. Novel repression of Kcc2 transcription by REST–RE-1 controls developmental switch in neuronal chloride. *J Neurosci*. 2009;29(46):14652-14662.
6. Engberink AHOO, Meijer JH, Michel S. Chloride cotransporter KCC2 is essential for GABAergic inhibition in the SCN. *Neuropharmacology*. 2018;138:80-86.
7. Ganguly K, Schinder AF, Wong ST, Poo M. GABA itself promotes the developmental switch of neuronal GABAergic responses from excitation to inhibition. *Cell*. 2001;105(4):521-532.
8. McKay S, Ryan TJ, McQueen J, et al. The developmental shift of NMDA receptor composition proceeds independently of GluN2 subunit-specific GluN2 C-terminal sequences. *Cell Rep*. 2018;25(4):841-851.e4.
9. Rodenas-Ruano A, Chávez AE, Cossio MJ, Castillo PE, Zukin RS. REST-dependent epigenetic remodeling promotes the developmental switch in synaptic NMDA receptors. *Nat Neurosci*. 2012;15(10):1382-1390.
10. Mampay M, Sheridan GK. REST: an epigenetic regulator of neuronal stress responses in the young and ageing brain. *Front Neuroendocrinol*. 2019;53:100744.
11. Pozzi D, Lignani G, Ferrea E, et al. REST/NRSF-mediated intrinsic homeostasis protects neuronal networks from hyperexcitability. *EMBO J*. 2013;32(22):2994-3007.
12. Pecoraro-Bisogni F, Lignani G, Contestabile A, et al. REST-dependent presynaptic homeostasis induced by chronic neuronal hyperactivity. *Mol Neurobiol*. 2018;55(6):4959-4972.
13. Prestigio C, Ferrante D, Marte A, et al. REST/NRSF drives homeostatic plasticity of inhibitory synapses in a target-dependent fashion. *eLife*. 2021;10:1-34.
14. Centonze E, Marte A, Albini M, et al. Neuron-restrictive silencer factor/repressor element 1-silencing transcription factor (NRSF/REST) controls spatial K^+ buffering in primary cortical astrocytes. *J Neurochem*. 2023;165(5):701-721.
15. Jensen BL, Persson PB. Good publication practice in physiology 2021. *Acta Physiol*. 2022; e13741. doi:10.1111/apha.13741
16. Nechiporuk T, McGann J, Mullendorff K, et al. The REST remodeling complex protects genomic integrity during embryonic neurogenesis. *eLife*. 2016;5(January 2016):e09584.
17. Chan KY, Jang MJ, Yoo BB, et al. Engineered AAVs for efficient noninvasive gene delivery to the central and peripheral nervous systems. *Nature Neuroscience*. 2017;20(8):1172-1179.
18. Kaeser PS, Deng L, Wang Y, et al. RIM proteins tether Ca2+ channels to presynaptic active zones via a direct PDZ-domain interaction. *Cell*. 2011;144(2):282-295.
19. McClure C, Cole KLH, Wulff P, Klugmann M, Murray AJ. Production and Titering of recombinant adeno-associated viral vectors. *J Vis Exp*. 2011;57: e3348. doi:10.3791/3348
20. Natali G, Michetti C, Krawczun-Rygmaczewska A, Floss T, Cesca F, Benfenati F. Conditional knockout of REST/NRSF in

excitatory neurons reduces seizure susceptibility to chemical kindling. *Front Cell Neurosci*. 2023;17: 1267609. doi:10.3389/fncel.2023.1267609
21. Shimada T, Yamagata K. Pentylenetetrazole-induced kindling mouse model. *J Vis Exp*. 2018;136: 56573. doi:10.3791/56573
22. Prestigio C, Ferrante D, Valente P, et al. Spike-related electrophysiological identification of cultured hippocampal excitatory and inhibitory neurons. *Mol Neurobiol*. 2019;56(9):6276-6292.
23. Valente P, Lignani G, Medrihan L, et al. Cell adhesion molecule L1 contributes to neuronal excitability regulating the function of voltage-gated Na^+ channels. *J Cell Sci*. 2016;129(9):1878-1891.
24. Kügler S, Kilic E, Bähr M. Human synapsin 1 gene promoter confers highly neuron-specific long-term transgene expression from an adenoviral vector in the adult rat brain depending on the transduced area. *Gene Ther*. 2003;10(4):337-347.
25. Bedbrook CN, Deverman BE, Gradinaru V. Viral strategies for targeting the central and peripheral nervous systems. *Annu Rev Neurosci*. 2018;41(1):323-348.
26. Carminati E, Buffolo F, Rocchi A, Michetti C, Cesca F, Benfenati F. Mild inactivation of RE-1 silencing transcription factor (REST) reduces susceptibility to Kainic acid-induced seizures. *Front Cell Neurosci*. 2020;13(January):1-10.
27. O'Brien RJ, Kamboj S, Ehlers MD, Rosen KR, Fischbach GD, Huganir RL. Activity-dependent modulation of synaptic AMPA receptor accumulation. *Neuron*. 1998;21(5):1067-1078.
28. Shao L-R, Dudek FE. Changes in mIPSCs and sIPSCs after Kainate treatment: status epilepticus–induced neuronal loss or direct activation of Kainate receptors? *J Neurophysiol*. 2006;96(2):961-962.
29. Butler-Ryan R, Wood IC. The functions of repressor element 1-silencing transcription factor in models of epileptogenesis and post-ischemia. *Metab Brain Dis*. 2021;36(6):1135-1150.
30. McClelland S, Brennan GP, Dubé C, et al. The transcription factor NRSF contributes to epileptogenesis by selective repression of a subset of target genes. *eLife*. 2014;3:e01267.
31. Hansen SL, Sperling BB, Sánchez C. Anticonvulsant and antiepileptogenic effects of GABAA receptor ligands in pentylenetetrazole-kindled mice. *Prog Neuro-Psychopharmacology Biol Psychiatry*. 2004;28(1):105-113.
32. Pitkänen A, Buckmaster PS, Galanopoulou AS, Moshé SL. *Models of Seizures and Epilepsy*. 2nd ed. Academic Press Inc; 2017.
33. Chang BS, Lowenstein DH. Epilepsy. *N Engl J Med*. 2003;349(13):1257-1266.
34. Holmes GL, Ben-Ari Y. The neurobiology and consequences of epilepsy in the developing brain. *Pediatr Res*. 2001;49(3):320-325.
35. Turrigiano G. Homeostatic synaptic plasticity: local and global mechanisms for stabilizing neuronal function. *Cold Spring Harb Perspect Biol*. 2012;4(1):a005736.
36. Lignani G, Baldelli P, Marra V. Homeostatic plasticity in epilepsy. *Front Cell Neurosci*. 2020;14:197.
37. Qiu Y, Neill NO, Maffei B, et al. On-demand cell-autonomous gene therapy for brain circuit disorders. *Science*. 2022;532(November):523-532.
38. Baldelli P, Meldolesi J. The transcription repressor REST in adult neurons: physiology, pathology, and diseases. *eNeuro*. 2015;2(4):ENEURO.0010-ENEU15.2015.
39. Turrigiano GG, Nelson SB. Homeostatic plasticity in the developing nervous system. *Nat Rev Neurosci*. 2004;5(2):97-107.
40. Samokhina E, Samokhin A. Neuropathological profile of the pentylenetetrazol (PTZ) kindling model. *Int J Neurosci*. 2018;128(11):1086-1096.
41. Hu X-L, Cheng X, Cai L, et al. Conditional deletion of NRSF in forebrain neurons accelerates epileptogenesis in the kindling model. *Cereb Cortex*. 2011;21(9):2158-2165.
42. Liu M, Sheng Z, Cai L, Zhao K, Tian Y, Fei J. Neuronal conditional knockout of NRSF decreases vulnerability to seizures induced by pentylenetetrazol in mice. *Acta Biochim Biophys Sin Shanghai*. 2012;44(6):476-482.

SUPPORTING INFORMATION

Additional supporting information can be found online in the Supporting Information section at the end of this article.

How to cite this article: Vitale C, Natali G, Cerullo MS, et al. The homeostatic effects of the RE-1 silencing transcription factor on cortical networks are altered under ictogenic conditions in the mouse. *Acta Physiol*. 2024;240:e14146. doi:10.1111/apha.14146